



1 Variability, timescales, and non-linearity in climate responses to
2 black carbon emissions

3

4

5 Yang Yang^{1*}, Steven J. Smith^{2*}, Hailong Wang¹, Catrin M. Mills¹, Philip J. Rasch¹

6

7

8

9 ¹Atmospheric Sciences and Global Change Division, Pacific Northwest National
10 Laboratory, Richland, Washington, USA

11 ²Joint Global Change Research Institute, Pacific Northwest National Laboratory,
12 College Park, Maryland, USA

13

14

15

16

17

18 *Correspondence to yang.yang@pnnl.gov and ssmith@pnnl.gov



19 **Abstract**

20 Black carbon (BC) particles exert a potentially large warming influence on the
21 Earth system. Reductions in BC emissions have attracted attention as a possible
22 means to moderate near-term temperature changes. For the first time, we evaluate
23 regional climate responses, non-linearity, and short-term transient responses to BC
24 emission perturbations in the Arctic, mid-latitudes, and globally based on a
25 comprehensive set of emission-driven experiments using the Community Earth
26 System Model (CESM). Surface temperature responses to BC emissions are
27 complex, with surface warming over land from mid-latitude BC perturbations partially
28 offset by ocean cooling. Climate responses do not scale linearly with emissions.
29 While stronger BC emission perturbations have a higher burden efficiency, their
30 temperature sensitivity is lower. BC impacts temperature much faster than
31 greenhouse gas forcing, with transient temperature responses in the Arctic and
32 mid-latitudes approaching a quasi-equilibrium state with a timescale of 2–3 years. We
33 find large variability in BC-induced climate changes due to background model noise.
34 As a result, perturbing present-day BC emission levels results in no discernible net
35 global-average surface temperature signal. In order to better understand the climatic
36 impacts of BC emissions, both the drivers of non-linear responses and response
37 variability need to be assessed across climate models.

38



39 **1. Introduction**

40 Black carbon (BC) aerosol, emitted from incomplete combustion, may be the
41 second strongest positive anthropogenic climate forcing following carbon dioxide,
42 which drew attentions for climate mitigation from reducing BC emissions (Jacobson,
43 2004; Shindell et al., 2012; Bond et al., 2013; Smith and Mizrahi, 2013). The
44 relationship between forcing and surface temperature changes caused by BC is
45 complex and forcing is not a reliable indicator of the climatic impact of BC emissions
46 (Stjern et al., 2017). BC absorbs solar radiation within the atmospheric column
47 thereby warming the atmosphere with an influence on surface temperature that
48 depends on its vertical location. At high altitudes, BC cools the surface by absorbing
49 solar radiation (i.e., blocking it from reaching the surface) (Ramanathan and
50 Carmichael, 2008), while BC at low altitudes warms the surface through diabatic
51 heating (Ban-Weiss et al., 2012). In addition, heating the atmosphere and cooling the
52 surface can increase atmospheric stability and therefore affect cloud formation,
53 lifetime, and dynamical processes (Koren et al., 2004; McFarquhar and Wang, 2006;
54 Koch and Del Genio, 2010). Through transformation from hydrophobic aggregates to
55 hydrophilic particles coated with water-soluble substances (i.e., aging processes), BC
56 can become cloud-nucleating particles (Oshima et al., 2009), alter cloud
57 microphysical processes, and suppress precipitation (Boucher et al., 2013).
58 BC-induced warming or cooling can increase or decrease surface evaporation,
59 resulting in further changes in precipitation and cloud formation (McFarquhar and
60 Wang, 2006; Andrews et al., 2010; Ming et al., 2010; Ban-Weiss et al., 2012;



61 Kvalevåg et al., 2013). BC can also decrease surface albedo through deposition on
62 snow and ice, which is especially important to the climate at high latitudes and,
63 particularly the Arctic (Flanner et al., 2007; Qian et al., 2014) as snow/ice-albedo
64 effects are strong there. Taken together, these processes result in interactions
65 between BC and the atmosphere that can ultimately alter the net impact of BC on
66 climate, which have been termed rapid adjustments (Stjern et al., 2017).

67 Studies found that increases in BC emissions may contribute to the amplification
68 of Arctic warming directly by absorbing solar radiation in the atmosphere and
69 indirectly by reducing surface albedo through deposition on snow and ice (Flanner et
70 al., 2007; Qian et al., 2014). Flanner (2013) highlighted the importance of BC vertical
71 location in Arctic climate responses, with surface warming (cooling) due to BC in the
72 lower (upper) troposphere. In addition, BC outside the Arctic can influence the Arctic
73 climate through changing poleward heat transport. With BC snow/ice-albedo effect
74 excluded, Shindell and Faluvegi (2009) modeled an Arctic surface warming (cooling)
75 due to reducing (enhancing) mid-latitude BC atmospheric concentrations. Sand et al.
76 (2013a) found that this was due to the increased northward heat transport into the
77 Arctic. However, in another study where BC emissions were perturbed instead of
78 concentrations, Sand et al. (2013b) reported a decrease in northward heat transport
79 due to increases in mid-latitude BC emissions and suggested that the heating effect
80 of BC transported to the Arctic dominated the Arctic heating in the mid-latitude
81 perturbation simulation, leading to the opposite direction of atmospheric heat
82 transport compared to the concentration-driven perturbations. They also found that



83 increases in both BC emission and BC concentration in the Arctic atmosphere may
84 weaken poleward heat transport due to increasing Arctic temperature driven by BC
85 heating in the atmosphere and on snow and ice surfaces. Therefore, understanding
86 the Arctic climate impact of regional BC emissions is important for the Arctic climate
87 mitigation (Sand et al., 2016).

88 In order to archive a statistically significant signal of Arctic surface temperature
89 responses to BC emissions, Sand et al. (2013b) scaled present-day BC emissions
90 within the Arctic by a factor of 150 and emissions from mid-latitudes by a factor of 9,
91 respectively, in the NorESM model with BC snow/ice-albedo effects included. They
92 found that emissions of BC within the Arctic have an Arctic surface temperature
93 response 5 times larger than those from mid-latitudes and attributed it to BC
94 snow/ice-albedo feedbacks. The impact of BC emission perturbations on
95 mid-latitudes were not examined in that study, which we do in this work to contrast
96 the impact of BC on the Arctic with mid-latitudes.

97 Much of the previous work on BC has used atmosphere-only models or
98 prescribed BC concentrations (Hansen et al., 2005; Ming et al., 2010; Ban-Weiss et
99 al., 2012; Sand et al., 2013a), which artificially reduces variability in model results.
100 Results qualitatively differ between prescribed BC-concentration and emission-driven
101 simulations with coupled models (Sand et al., 2013a,b, 2015). A previous study using
102 coupled models found that the BC response in three of these models showed high
103 variability and inconsistency in the net sign of the responses to present-day BC
104 emissions both between models and even between ensemble members from the



105 same model (Baker et al., 2015). Stjern et al. (2017) investigated climate responses
106 to a tenfold increase in present-day anthropogenic BC concentrations or emissions
107 using five concentration-driven and four emission-driven global climate models. They
108 found that low-level cloud amounts increase, while higher-level clouds are diminished
109 for all models, which is dominated by rapid adjustments. The negative rapid
110 adjustments from changing clouds dampened positive instantaneous radiative forcing
111 of BC at the TOA, leading to a relatively small global warming. However, this study
112 did not consider response variability or non-linearity of responses. We note that the
113 model used in ours study contains a different aerosol treatment than the model used
114 in Stjern et al. (2015).

115 To better understand the impacts of BC on climate, we present a comprehensive
116 analysis using a set of coupled simulations that examine regional climate responses,
117 non-linearity, and short-term transient climate responses to BC emission
118 perturbations. We focus in particular on the Arctic and also variability to assess if
119 climate responses to BC emission changes are likely to be discernable. Only
120 combustion and process-based anthropogenic BC emissions are perturbed, given
121 that the net global climate impact of open burning emissions has been assessed to be
122 small due to their high organic carbon fraction. A summary of key results is provided
123 below.

124

125 **2. Methods**

126 **2.1 Model description**



127 Here we use the fully coupled CESM (Community Earth System Model; Hurrell et
128 al., 2013) to simulate climate responses to BC emission perturbations. In
129 CAM5-MAM4 (Community Atmosphere Model version 5), the atmospheric
130 component of CESM, mass and number concentrations of aerosols are predicted
131 within four lognormal modes (i.e., Aitken, accumulation, coarse, and primary carbon
132 mode) of the modal aerosol module (MAM4; Liu et al., 2016). BC is emitted into the
133 primary-carbon mode and aged into the accumulation mode when coated with sulfate
134 or secondary organic aerosol. Particles in the accumulation mode, including BC and
135 other species, can serve as cloud condensation nuclei and have microphysical
136 effects on stratiform clouds and precipitation. The model physically treats
137 aerosol-cloud interactions using two-moment stratiform cloud microphysics, which
138 predicts number concentrations and mixing ratios of cloud water and ice (Morrison
139 and Gettelman, 2008; Gettelman et al., 2010). Activation of stratiform cloud droplets
140 is based on the scheme of Abdul-Razzak and Ghan (2000). In addition to the
141 standard treatments of aerosol-cloud interactions, we also include a set of
142 modifications that improves the simulation of aerosol wet scavenging and convective
143 transport (Wang et al., 2013). Although aerosols have no microphysical impact on
144 convective clouds, BC induced atmospheric heating can affect the ambient
145 temperature and convection. Convective precipitation can scavenge and remove
146 aerosols. The CAM5 model has been extensively evaluated in simulating
147 concentration, deposition, vertical profile and optical properties of BC in previous



148 studies (Wang et al., 2013; Wang et al., 2015; Zhang et al., 2015a,b; Liu et al., 2016;
149 Yang et al., 2017, 2018a,b).

150 In our model simulations, atmospheric radiative transfer is calculated twice with
151 BC included and excluded, respectively. The changes in direct radiative effect and
152 cloud radiative effect induced by BC perturbation are calculated as $\Delta(F_{\text{clear}} - F_{\text{clear, clean}})$
153 and $\Delta(F_{\text{clean}} - F_{\text{clear, clean}})$, respectively, where F_{clear} is the TOA flux calculated
154 neglecting scattering and absorption by clouds, F_{clean} is the TOA flux calculated
155 neglecting scattering and absorption by BC, $F_{\text{clear, clean}}$ is the TOA flux calculated
156 neglecting scattering and absorption by both clouds and BC, and Δ refers to the
157 differences between the control and one of the emission perturbed simulations (Ghan,
158 2013). Note that these quantities include the impact of slow responses and feedbacks
159 (e.g., changes in sea surface temperature and sea ice and feedbacks with clouds) so
160 are not strictly comparable to the conventional definition of radiative forcing (Boucher
161 et al., 2013). The BC snow/ice-albedo effect on top of land and sea ice is included in
162 the model (Flanner et al., 2007; Yang et al., 2017, 2018c).

163 **2.2 Experimental configurations and emissions**

164 The following simulations are performed in this study. All insolation, greenhouse
165 gas concentrations and aerosol and precursor emissions, except BC, are fixed at
166 year 1850 levels, which include open burning emissions (van Marle et al., 2017).

167 The MID7X and ARC150X simulations use large emission perturbations to result
168 in signals large enough for detailed analysis. These regions are also particularly
169 important for BC impacts on the Arctic. The multipliers were selected following Sand



170 et al. (2013b) with the expectation that these would result in similar radiative
171 perturbations. This also allows a direct comparison to these previous results (Sand et
172 al., 2013b; Baker et al., 2015), which are also BC-emission simulations using a
173 coupled model with snow/ice-albedo feedbacks. The PD simulation then allows us to
174 evaluate the impact of present-day anthropogenic emissions.

- 175 1. PD: control simulation for BC in present-day conditions. BC emissions are
176 fixed at year 2010 (average of 2008–2012).
- 177 2. ARC150X: perturbed simulation to quantify the climate responses to Arctic BC
178 emissions. Same as PD except that year 2010 level anthropogenic BC
179 emissions over the Arctic (60–90°N) are scaled by a factor of 150.
- 180 3. MID7X: perturbed simulation to quantify the climate responses to mid-latitude
181 BC emissions. Same as PD except that year 2010 level anthropogenic BC
182 emissions over the mid-latitudes (28–60°N) are scaled by a factor of 7.
- 183 4. ARC75X: perturbed simulation to quantify non-linearity of climate responses to
184 Arctic BC emissions. Same as ARC150X except that Arctic BC emissions are
185 scaled by a factor of 75.
- 186 5. MID3.5X: perturbed simulation to quantify non-linearity of climate responses to
187 mid-latitude BC emissions. Same as MID7X except that mid-latitude BC
188 emissions are scaled by a factor of 3.5.
- 189 6. MID14X: perturbed simulation to quantify non-linearity of climate responses to
190 mid-latitudes BC emissions. Same as MID7X except that mid-latitude BC
191 emissions are scaled by a factor of 14.



192 7. PI: sensitivity simulation for BC in preindustrial conditions to compare results
193 with Baker et al. (2015). BC emissions are at year 1850 levels.
194 Both mass and number of BC emissions are perturbed proportionally. Each
195 simulation has one ensemble member for 100 years which are branched from year 81
196 of the PI simulation after 80 years spin-up, with the last 80 years used for most
197 analysis. Another four short-term ensemble members for 30 years are conducted
198 under both ARC150X and MID7X to examine the short-term transient climate
199 response to BC emissions. These are branched from years 96, 112, 120, and 140 of
200 PI simulation.
201 The CEDS (Community Emissions Data System) anthropogenic emissions
202 (Hoesly et al., 2018) (version 2017-05-18) that were developed for the CMIP6
203 (Coupled Model Intercomparison Project Phase 6) model experiments are used in our
204 simulations. Figure S1 shows spatial distribution of annual anthropogenic BC
205 emissions for year 2010 (average of 2008–2012) and the regions for BC emission
206 perturbation. Over 60–90°N, anthropogenic BC emissions are mostly over the lower
207 latitude of the Arctic (60–70°N). Over the mid-latitudes, high BC emissions are mainly
208 located over eastern China. The annual total anthropogenic BC emission from the
209 Arctic in year 2010 is 0.08 Tg C yr⁻¹, with 70% contributed by energy sector. Scaled
210 by a factor of 150, ARC150X has 12.63 Tg C yr⁻¹ more BC emissions than the PD in
211 the Arctic. About 3.46 Tg C yr⁻¹ of BC is emitted from the mid-latitudes, with the
212 largest contribution from the residential sector (36%). With a scaling factor of 7,
213 MID7X includes an additional 20.74 Tg C yr⁻¹ of BC emission from mid-latitudes, as



214 compared to PD. Global annual anthropogenic BC for PD is $7.72 \text{ Tg C yr}^{-1}$, much
215 higher than $0.92 \text{ Tg C yr}^{-1}$ for PI.

216

217 **3. Regional climate responses to increases in Arctic and mid-latitude BC** 218 **emissions**

219 We first examine results from simulations with large perturbations of both Arctic
220 and mid-latitude BC emissions (ARC150X and MID7X). Our initial simulations
221 focused on these regions due to the potentially high sensitivity of the Arctic to BC
222 emissions. Figure 1 presents the increases in annual, zonal-mean BC concentrations
223 from ARC150X and MID7X simulations, as compared to PD. Both Arctic and
224 mid-latitude BC emissions lead to BC concentration increases in the entire Northern
225 Hemisphere, with Arctic emissions mainly impacting low altitudes within the Arctic. In
226 ARC150X, due to extremely low temperatures at the surface and therefore
227 temperature inversions and a transport barrier (so called Arctic front), increasing BC
228 concentrations are mainly located over low altitudes within the Arctic. In MID7X,
229 increased mid-latitude emissions produce large increases in BC concentrations
230 between 30° – 45° N. BC emitted over the mid-latitudes, which is lifted above the
231 boundary layer and transported at higher altitudes into the Arctic, leading to increased
232 concentrations of BC in the Arctic atmosphere. This spatial pattern is similar to those
233 in Sand et al. (2013b).

234 To explore the importance of additional emissions from different source regions to
235 the increase in BC column burdens, Table 1 summarizes BC burden efficiency, which



236 is defined as the changes in regional mean column burden of BC produced by per
237 unit emission change, calculated by differences between a perturbed simulation and
238 PD simulation. Over the Arctic, increases in Arctic local BC emissions lead to an
239 Arctic burden efficiency of $0.425 \pm 0.024 \text{ mg m}^{-2} (\text{Tg yr}^{-1})^{-1}$. The burden efficiency of
240 mid-latitude emissions over the mid-latitudes is $0.191 \pm 0.004 \text{ mg m}^{-2} (\text{Tg yr}^{-1})^{-1}$, less
241 than half of the efficiency of Arctic emission on Arctic burden due to lower
242 precipitation and frequent temperature inversion in the Arctic compared to
243 mid-latitudes. While the relative impact of mid-latitude emissions on the Arctic burden
244 efficiency ($0.106 \pm 0.004 \text{ mg m}^{-2} (\text{Tg yr}^{-1})^{-1}$) is smaller than either of the above
245 efficiencies, the 30 times larger total emissions from mid-latitudes are likely to
246 dominate column burden contributions.

247 Table 1 also summarizes the changes in BC direct radiative effect, cloud radiative
248 effect, and snow/ice-albedo forcing induced by these large BC perturbations. Note
249 that these values include feedback effects from the coupled system, so are not
250 comparable to conventionally defined radiative forcing values. The albedo change
251 due to BC deposition on snow and ice is responsible for a significant increase in
252 Arctic surface forcing in both perturbations, with far smaller changes per unit emission
253 in mid-latitudes. Positive changes in direct radiative effect are offset by negative
254 changes in cloud radiative effect from increases in low cloud in the Arctic and
255 decreases in mid-level and high cloud over the mid-latitudes, similar to previous
256 results with a tenfold increase in present-day anthropogenic BC emissions (Stjern et
257 al., 2017).



258 Forcing efficiencies of direct radiative effect, cloud radiative effect and
259 snow/ice-albedo forcing (i.e., forcings produced by per unit emission change) are also
260 summarized in Table 1. Over the Arctic, local emissions from the Arctic have 2–4
261 times higher forcing efficiencies than emissions from the mid-latitudes, suggesting
262 higher impacts of a unit Arctic BC emission change to Arctic energy balance. Over the
263 mid-latitudes, although forcing efficiencies of direct radiative effect and cloud radiative
264 effect for Arctic emissions are 2–3 times lower than mid-latitude emissions, the
265 snow/ice-albedo forcing efficiencies are similar between Arctic and mid-latitude
266 emissions.

267 The annual mean surface air temperature responses in ARC150X show a
268 significant warming over both the Arctic and mid-latitudes (Figure 2). MID7X shows
269 temperature increases over the Arctic and most of the mid-latitude land regions, while
270 surface temperature decreases over some oceanic and coastal areas. The presence
271 of areas with both surface warming and cooling decreases the net average
272 temperature change over mid-latitudes.

273 Due to the increased atmospheric absorption from BC, northward heat transport
274 for both perturbations decreases (Figure 3), consistent in sign with the results of Sand
275 et al. (2013b). The increases in temperature but decreases in net northward heat
276 transport indicate that the heating induced by changes in BC direct radiative effect
277 and BC snow/ice-albedo forcing dominate the overall BC-induced changes in energy
278 balance over the Arctic and mid-latitudes.



279 Arctic emissions are more efficient at impacting Arctic surface air temperatures
280 with an Arctic temperature sensitivity to Arctic emissions ($0.169 \pm 0.052 \text{ K (Tg yr}^{-1}\text{)}^{-1}$)
281 seven times as large as the Arctic temperature sensitivity to mid-latitude emissions
282 ($0.023 \pm 0.038 \text{ K (Tg yr}^{-1}\text{)}^{-1}$). Mid-latitude emissions, however, are likely to have a
283 larger present-day impact overall due to their 30 times larger present-day emission
284 levels. Note that, the Arctic temperature sensitivities are about 30% and 50% smaller
285 than those found in the coupled NorESM model experiments of Sand et al. (2013b)
286 for Arctic and mid-latitude emission perturbation simulations, respectively, probably
287 due to different model parameterizations and/or different vertical profile of BC driving
288 the net effect of BC impact on Arctic surface temperature (Flanner, 2013).

289 The vertical distribution of annual, zonal mean temperature responses (Figure 4)
290 shows that the ARC150X leads to a strong warming from the surface to 400 hPa over
291 the Arctic and between 40° – 60° N. In MID7X, although the zonal mean surface
292 temperature response is relatively weak compared to ARC150X, a significant
293 warming is found in mid-latitudes between 500 and 200 hPa. BC transported from
294 mid-latitudes into the Arctic at high altitudes results in temperature increases between
295 400 and 300 hPa over the Arctic. These changes in temperature pattern can change
296 the stability of the atmosphere and impact atmospheric circulation.

297 Figure 5 shows changes in annual mean meridional circulation. Increases in BC
298 emissions over both the Arctic and mid-latitudes exert anomalous upward motions in
299 the Arctic and downward motions over the mid-latitudes, but for different reasons. In
300 ARC150X, stronger warming at the Arctic surface, compared to high altitudes, likely



301 due to the BC snow/ice-albedo effect, produces anomalous upward motions in the
302 Arctic and compensating downward motions between 50°–60°N. In MID7X, the
303 stronger BC warming at higher altitudes in mid-latitudes increases the atmospheric
304 stability and leads to strong anomalous downward motions between 40°–60°N and
305 compensating upward motions over the Arctic and 10°–30°N (Johnson et al., 2004).
306 Increasing surface temperature and anomalous upward motion over the Arctic can
307 weaken the Arctic front, and the anomalous downward motion over the mid-latitudes
308 favors air stagnation.

309 Because of the anomalous downward motions over mid-latitudes in both
310 ARC150X and MID7X, high and/or mid-level cloud fraction decrease over
311 mid-latitudes (Figure 6). Due to slow feedbacks from increases in surface
312 temperature in the Arctic (Figure 2) and decreases in snow and sea ice, low cloud
313 fraction increases in the Arctic for both ARC150X and MID7X. The increases in low
314 cloud over mid-latitude oceans, which cause the cooling noted above, are due to
315 rapid adjustments that the free-tropospheric BC heating reduces mixing with dry air
316 above the BC layer and increases the amount of marine stratocumulus (Johnson et
317 al., 2004; Sand et al., 2013a; Stjern et al., 2017).

318 Figure 7 shows changes in the total precipitation rate for the perturbed
319 simulations. Increases in Arctic and mid-latitude BC emissions lead to significant
320 decreases in precipitation over 60°N and 30–50°N, respectively, in correspondence
321 with anomalous downward motions (Figure 5) and decreases in mid-level and high
322 clouds (Figure 6) over these regions. Averaged over the Arctic and mid-latitudes,



323 changes in precipitation are weak, compared to uncertainties, except for the
324 mid-latitude precipitation response to BC emitted from mid-latitudes. The mid-latitude
325 precipitation sensitivity is $-7.67 (\pm 3.34) \mu\text{m day}^{-1} (\text{Tg yr}^{-1})^{-1}$ for MID7X. Another
326 feature of the precipitation response is related to a northward shift in the ITCZ
327 (Intertropical Convergence Zone) in MID7X, which is consistent with the
328 hemispherically asymmetric warming pattern driven by increases in mid-latitude BC
329 emissions (Hwang et al., 2013; Baker et al., 2015).

330 Both ARC150X and MID7X show significant decreases by 13% and 3%,
331 respectively, in fractional area covered by sea ice over the Arctic, as compared to PD
332 (Figure S2). The snow depth over land also decreases, especially over Greenland.
333 The water equivalent snow depth averaged over Arctic land decreases by 5.0 cm (27%
334 relative to PD) and 0.8 cm (4%), respectively, for ARC150X and MID7X.

335

336 **4. Non-linearity of climate responses.**

337 We also evaluated the linearity of these responses by testing different emission
338 perturbation sizes. Figure 8 shows burden efficiencies, temperature and precipitation
339 sensitivities from simulations with Arctic BC emissions scaled by 75 and 150,
340 respectively, and mid-latitude BC emissions scaled by 3.5, 7 and 14, respectively,
341 and Table 2 summarized these values. Stronger emission perturbations have a
342 higher burden efficiency. Over the Arctic, this is caused by anomalous Arctic upward
343 motions that weaken the Arctic front, lifting BC higher and leading to a longer BC
344 lifetime together with easier transport into the Arctic (Figure S3). Over mid-latitudes,



345 anomalous mid-latitude downward motions favor stagnation, which in turn
346 accumulates more BC in the atmosphere, together with decrease in precipitation (and
347 wet removal rate), contributing to increases in burden efficiency.

348 Despite this higher burden efficiency, the efficiency of direct radiative effect
349 decreases slightly. This is because strong BC perturbations lead to more BC
350 suspended in the atmosphere. More BC increases the attenuation of the transmitted
351 radiation, leading to a decrease in efficiency of BC light absorption in the lower
352 atmosphere and leading to a lower efficiency of direct radiative effect for a stronger
353 BC emissions perturbation.

354 The temperature sensitivity is lower for stronger emission perturbations for both
355 mid-latitude and Arctic BC. The BC snow/ice-albedo effect is found to be the most
356 important factor in influencing Arctic temperature (Sand et al., 2013b). Larger
357 temperature increases from stronger BC emission perturbations speed up sea ice
358 and snow melt, leading to a weaker annual mean snow/ice-albedo effect per unit BC
359 emission for both Arctic and mid-latitudes. Therefore, the BC snow/ice-albedo effect
360 is more efficient for weaker emission perturbations, i.e., $0.151 (\pm 0.011)$ vs. 0.099
361 (± 0.006) ($\text{W m}^{-2} (\text{Tg yr}^{-1})^{-1}$) for ARC75X and ARC150X and $0.026 (\pm 0.002)$ vs. 0.020
362 (± 0.002) ($\text{W m}^{-2} (\text{Tg yr}^{-1})^{-1}$) for MID7X and MID14X of Arctic BC snow/ice-albedo
363 forcing efficiencies. Together with lower efficiency of direct radiative effect, these
364 explain the lower temperature sensitivity for stronger emission perturbation. The
365 non-linearity in snow-ice feedback relative to emissions size appears to be the
366 primary driver of surface temperature response non-linearity in these results.



367 Sand et al. (2015) simulated climate responses to BC in NorESM with
368 present-day emissions multiplied by 25 and reported that the changes in TOA net
369 shortwave flux was $7.5 (\pm 0.3) \text{ W m}^{-2}$ relative to preindustrial conditions and the
370 temperature response was $1.2 (\pm 0.1) \text{ K}$. If we assume a linear emission-response
371 relationship, present-day BC would cause an inferred shortwave flux and surface
372 temperature changes of $0.312 (\pm 0.013) \text{ W m}^{-2}$ and $0.050 (\pm 0.004) \text{ K}$ in Sand et al.
373 (2015), much lower than the 0.552 W m^{-2} and 0.141 K found in Baker et al. (2015) for
374 a present-day BC emission perturbation. Note that the change in shortwave flux is not
375 proportional to the surface temperature change, further emphasizing that forcing is not
376 a good predictor of surface temperature change for BC. This comparison is consistent
377 with our finding that temperature sensitivity is lower for stronger BC emission
378 perturbation. We note, however, that emission datasets with different spatial
379 distributions and seasonality were used in those two experiments (because of this the
380 difference in global emissions between the two experiments is about 17, not 25 times).
381 While this might impact the magnitude of model responses, it is unlikely to change the
382 overall conclusion of a substantially different temperature response to current-day
383 emissions as compared to a 17 times larger BC perturbation.

384 The mid-latitude shows a stronger precipitation sensitivity for a stronger
385 perturbation, comparing MID7X and MID14X, which is consistent with the higher
386 burden efficiency. This is in the opposite direction to the surface temperature
387 sensitivity. Variability in MID3.5X is larger than the mean value for both temperature
388 and precipitation sensitivity, which highlights the challenge of testing differences for



389 smaller BC perturbation magnitudes. Note that the impact of BC on clouds and
390 precipitation is uncertain, especially in the Arctic, due to the limited treatment of Arctic
391 clouds in climate models (McFarquhar et al., 2011). These results suggest that in
392 order to examine the climate responses to BC emissions in short-term climate model
393 simulations, a large emission perturbation is needed to get a clear signal, but
394 non-linearity of the responses also needs to be evaluated.

395

396 **5. Short-term transient climate responses**

397 To assess the short-term transient climate responses to BC emissions, Figure 9
398 shows surface temperature responses to BC emissions from ARC150X and MID7X
399 for the first 30 years averaged over five short ensemble members. We also show a
400 numerical fit to the short-term transient response using a Hamiltonian Monte Carlo
401 technique (Betancourt, 2017). We fit to the following form:

$$402 \quad T_{\text{ave}} (1 - e^{-t/\tau})$$

403 where we have constrained the fit to converge to the long-term average
404 temperature response (T_{ave}) by our observation that there is no detectable long-term
405 trend after the initial transient period.

406 Over both the Arctic and mid-latitudes, transient temperature responses quickly
407 approach a quasi-equilibrium state. Transient timescales (τ) for the ARC150X
408 perturbation were estimated to be 2.7 (2.0, 3.4) years, while the mid-latitude
409 timescales for the ARC150X and MID7X perturbations were 1.8 (1.1, 2.2) and 2.9
410 (1.2, 4.2) years respectively (brackets provide 10-90% fitting intervals). The Arctic



411 response to MID7X was too noisy to provide a fit. These timescales are shorter than
412 in a global BC perturbation experiment (Sand et al., 2015), which is expected as
413 ocean thermal inertia would play a larger role globally as compared to the Northern
414 Hemisphere or Arctic. The BC response timescales here are not only shorter than
415 those seen from changes in CO₂ concentrations in GCMs (Geoffroy et al., 2013), but
416 there is also no long-term temperature increase after the initial transient period.

417 Note that the average of even five ensemble members shows oscillatory behavior
418 due to the imposition of a step BC emission perturbation. In future work, a phased-in
419 perturbation might result in a cleaner signal for determining the initial response
420 time-scale.

421

422 **6. Climate responses to present-day anthropogenic BC emissions**

423 Baker et al. (2015) showed that the climate responses to BC emissions had very
424 large uncertainties based on results from four global models. Here, we also quantified
425 the impact of present-day anthropogenic BC emissions (Figure 10) by comparing a
426 present-day (PD) and pre-industrial (PI) simulation conducted with the
427 CESM-CAM5-MAM4 model used in this work. PD emissions produce statistically
428 significant surface air temperature changes over only limited regions in the Northern
429 Hemisphere. Decreased temperatures are found over eastern China, South Asia,
430 North Atlantic Ocean, and North American Arctic, partly due to cloud changes driven
431 by BC rapid adjustments. Increased temperatures are found over the Tibetan Plateau,



432 Greenland and high-latitude land regions likely because of the BC snow/ice-albedo
433 effect (Figure S4).

434 The spatial pattern is similar to that from the ECHAM6-HAM2 in Baker et al.
435 (2015). Although CESM-CAM5-MAM4 also includes the BC snow/ice-albedo effect,
436 we do not see the strong warming produced in NorESM under present-day BC
437 emissions. In Baker et al. (2015), NorESM had a global net TOA shortwave forcing
438 efficiency of $0.076 \text{ W m}^{-2} (\text{Tg yr}^{-1})^{-1}$, nominally higher than $0.043 \pm 0.073 \text{ W m}^{-2} (\text{Tg}$
439 $\text{yr}^{-1})^{-1}$ calculated in this study with CESM-CAM5-MAM4, although the difference is
440 well within one standard deviation. Longer model runs would be needed to determine
441 if BC snow/ice-albedo effect is significantly different in CESM and NorESM. In
442 addition, there may be a small contribution from a shorter BC lifetime (7.22 days in
443 CESM-CAM5-MAM4 Vs. 7.82 days in NorESM) that might also help explain the
444 weaker warming in CESM-CAM5-MAM4 as compared to NorESM.

445 We find that variability is substantial in our experiments. Large-scale surface
446 temperature change from current-day BC emissions is statistically indistinguishable
447 from zero ($0.006 \pm 0.238 \text{ K}$ globally and $0.020 \pm 0.346 \text{ K}$ for land only). The global
448 temperature response is within the range of -0.085 to 0.152 K from the four models in
449 Baker et al. (2015). Even in the large MID7X perturbation, variability is still fairly large
450 relative to the signal ($0.45 \pm 0.27 \text{ K}$ for mid-latitude temperate change) and would
451 overwhelm any large-scale signal for more realistic perturbation sizes. Similarly, while
452 the mid-latitude precipitation response to mid-latitude BC emissions is strong for a
453 MID7X perturbation, this would be difficult to detect for a present-day perturbation.



454

455 **7. Conclusions and discussions**

456 BC has been estimated to potentially have one of the largest positive (warming)
457 anthropogenic forcing influences. As a result, there has been substantial scientific
458 and policy attention focused on the potential for BC to moderate climate change in the
459 near-term. In this study, for the first time, we conduct a comprehensive set of
460 emission-driven experiments using a leading coupled climate model (CESM). With a
461 comprehensive set of experiments, we examined regional climate responses,
462 non-linearity, and short-term transient responses to BC emission perturbations in the
463 Arctic, mid-latitudes, and globally.

464 With increases in mid-latitude BC emissions, surface air temperature increases
465 over land, while it decreases over oceanic and coastal areas. Increases in Arctic BC
466 emissions lead to a significant warming over both the Arctic and mid-latitudes.
467 Increases in Arctic and mid-latitude BC emissions also decrease precipitation over
468 60°N and 30–50°N, respectively. Arctic emissions are more efficient in influencing
469 Arctic surface air temperatures compared to mid-latitude emissions, with an Arctic
470 temperature sensitivity to Arctic emissions seven times as large as that to mid-latitude
471 emissions.

472 Climate responses do not scale linearly with emissions. While stronger BC
473 emission perturbations have a higher burden efficiency, efficiencies of
474 snow/ice-albedo forcing and direct radiative effect are lower, leading to a lower
475 temperature sensitivity for stronger BC emission perturbation. BC impacts



476 temperature much faster than greenhouse gas forcing, with transient temperature
477 responses in the Arctic and mid-latitudes approaching a quasi-equilibrium state with a
478 timescale of 2–3 years.

479 We find large variability in BC-induced climate changes. Baker et al. (2015)
480 provided error bars of global temperature response for different model in Figure 4a of
481 their study. We note, however, that the error bars in Baker et al. are underestimated
482 because of their assumption of independence of all annual data points (note their use
483 of $1\sigma/\sqrt{N}$ in their error bars for Figure 4). Climate model surface temperatures are
484 strongly correlated over short time scales, which means that instead of the number of
485 data points, a more appropriate measure is the effective number of independent data
486 points (N_{eff}). The 100-year model runs examined here do not provide enough data for
487 this calculation. (Note that we were able to estimate N_{eff} for the 300-year CESM
488 control run from CMIP5, which indicates that runs around 3 times as long as those
489 presented here may be necessary). We, therefore, present standard deviation as a
490 metric of variance.

491 The standard deviation (SD) of global mean surface temperature in PI, PD, and in
492 all of our perturbed simulations is around 0.17–0.19 K, indicating that the dominant
493 source of temperature variability is probably due to internal climate variability or
494 model noise. The SD for temperature responses in perturbed simulations relative to
495 PD are in ranges of 0.24–0.26, roughly 1.4 times the control run temperature
496 variability. This is in the expectation from subtracting two independent Gaussian
497 noise distributions. While there could be an additional contribution to variability from



498 BC-climate interactions, this appears to be small in this case given the relatively small
499 surface temperature response to BC. We also observe large variability in cloud
500 radiative effects, which we note may be impacted by interactions with BC.

501 While we have demonstrated non-linear responses at high emission levels, this
502 non-linearity is not sufficient to produce statistically significant global temperature
503 changes from present-day BC emissions in this model. Such non-linearities mean
504 that the implications of large BC emission perturbation experiments, such as recent
505 tenfold BC experiments⁵ for present-day conditions are unclear. While
506 snow/ice-albedo feedbacks appear to dominate the non-linear relationship in these
507 results, this may not be the case in other models.

508 Our results point to the importance of better quantifying the variability in BC
509 responses in the Earth system. We note that in the one model with a consistent PD-PI
510 signal in a set of recent PD-PI BC experiments (NorESM1-M), the size of that signal
511 is still smaller than the variability found here, based on similar SD in Arctic
512 temperature change for the ARC150X simulations in the two models (compare Figure
513 S5 here with Figure 9 in Sand et al. (2013b)). If the global variability of BC response
514 in NorESM is also similar to that in CESM, then the global average temperature
515 change from NorESM (0.141 K) (Baker et al., 2015) is also much smaller than the SD
516 in CESM of 0.238 K. However, we do note that there was a fair degree of consistency
517 in temperature change signal in NorESM between two ensemble members (0.129 K
518 and 0.152 K). This may mean that variability in the global BC response in the
519 NorESM model could be smaller than seen in our results due to the stronger NorESM



520 BC temperature response. Longer simulations would likely be required to assess this.
521 While, compared to temperature or precipitation, aerosol burdens, BC direct radiative
522 effects and snow/ice-albedo forcings have much larger signal to noise ratios and can
523 be useful as diagnostics, BC forcing does not provide a reliable indicator of surface
524 temperature changes across models.

525 These indicate that even substantial BC emissions reductions from current levels
526 may lead to detectable surface temperature changes for only limited regions of the
527 globe. Our results have significant implications for near-term climate mitigation
528 associated with BC as well as global and regional climate attribution. We note that
529 regional climate sensitivities (RCS), used as an approximate approach to represent
530 the impact of BC (Collins et al., 2013; Sand et al., 2016), are generally evaluated
531 using model simulations with prescribed forcing or burdens (Shindell and Faluvegi,
532 2009), which artificially reduce response variability and imply a certainty in BC
533 responses that may not exist in reality. Variability within any given model run, which
534 has generally not been reported in current literature, is large relative to BC responses.
535 It is, therefore, not clear if current BC emission levels result in statistically significant
536 large-scale climatic changes. We suggest that impacts of BC on climate should be
537 expressed directly in terms of emissions not forcing, re-evaluated using coupled
538 models, and provided with measures of response variability, such as standard
539 deviation. In order to better assess the potential impact of changes in BC emissions it
540 is critical to quantify the non-linearity of BC response efficiencies with respect to



541 emission perturbation size in other models, as well as the causes of those
542 non-linearities.

543

544

545

546 ***Acknowledgments.***

547 This research is based on work that was supported by the Climate Change Division
548 of U.S. Environmental Protection Agency, and the U.S. Department of Energy (DOE),
549 Office of Science, Biological and Environmental Research as part of the Regional and
550 Global Climate Modeling program. The Pacific Northwest National Laboratory is
551 operated for DOE by Battelle Memorial Institute under contract
552 DE-AC05-76RLO1830. The National Energy Research Scientific Computing Center
553 (NERSC) provided computational support. Model results are available through
554 NERSC upon request.

555

556



557 **References**

558

559 Abdul-Razzak, H. and Ghan, S. J.: A parameterization of aerosol activation 2.

560 Multiple aerosol types, *J. Geophys. Res.*, 105, 6837–6844,

561 doi:10.1029/1999JD901161, 2000.

562

563 Andrews, T., Forster, P. M., Boucher, O., Bellouin, N., and Jones, A.: Precipitation,

564 radiative forcing and global temperature change, *Geophys. Res. Lett.*, 37,

565 L14701, doi:10.1029/2010GL043991, 2010.

566

567 Baker, L. H., Collins, W. J., Olivie, D. J. L., Cherian, R., Hodnebrog, Ø., Myhre, G.,

568 and Quaas, J.: Climate responses to anthropogenic emissions of short-lived

569 climate pollutants, *Atmos. Chem. Phys.*, 15, 8201–8216,

570 doi:10.5194/acp-15-8201-2015, 2015.

571

572 Ban-Weiss, G. A., Cao, L., Bala, G., and Caldeira, K.: Dependence of climate forcing

573 and response on the altitude of black carbon aerosols, *Clim. Dyn.*, 38, 897–911,

574 doi:10.1007/s00382-011-1052-y, 2012.

575

576 Betancourt, M.: A conceptual introduction to Hamiltonian Monte Carlo, arXiv preprint,

577 arXiv:1701.02434, 2017.

578

579 Bond, T. C., Doherty, S. J., Fahey, D. W., Forster, P. M., Berntsen, T., DeAngelo, B. J.,

580 Flanner, M. G., Ghan, S., Kärcher, B., Koch, D., Kinne, S., Kondo, Y., Quinn, P.

581 K., Sarofim, M. C., Schultz, M. G., Schulz, M., Venkataraman, C., Zhang, H.,

582 Zhang, S., Bellouin, N., Guttikunda, S. K., Hopke, P. K., Jacobson, M. Z., Kaiser,

583 J. W., Klimont, Z., Lohmann, U., Schwarz, J. P., Shindell, D., Storelvmo, T.,

584 Warren, S. G., and Zender, C. S.: Bounding the role of black carbon in the climate

585 system: A scientific assessment, *J. Geophys. Res.*, 118, 5380–5552,

586 doi:10.1002/jgrd.50171, 2013.

587

588 Boucher, O., Randall, D., Artaxo, P., Bretherton, C., Feingold, G., Forster, P.,

589 Kerminen, V.-M., Kondo, Y., Liao, H., Lohmann, U., Rasch, P., Satheesh, S. K.,

590 Sherwood, S., Stevens, B., and Zhang, X. Y.: Clouds and Aerosols, in: *Climate*

591 *Change 2013: The Physical Science Basis*, Contribution of Working Group I to

592 the Fifth Assessment Report of the Intergovernmental Panel on Climate Change,

593 edited by: Stocker, T. F., Qin, D., Plattner, G.-K., Tignor, M., Allen, S. K.,

594 Boschung, J., Nauels, A., Xia, Y., Bex, V., and Midgley, P. M., Cambridge

595 University Press, Cambridge, United Kingdom and New York, NY, USA, 571–658,

596 doi:10.1017/CBO9781107415324.016, 2013.

597

598 Collins, W. J., Fry, M. M., Yu, H., Fuglestedt, J. S., Shindell, D. T., and West, J. J.:

599 Global and regional temperature-change potentials for near-term climate forcers,



- 600 Atmos. Chem. Phys., 13, 2471–2485, <https://doi.org/10.5194/acp-13-2471-2013>,
601 2013.
602
- 603 Flanner, M. G.: Arctic climate sensitivity to local black carbon, *J. Geophys. Res.*
604 *Atmos.*, 118, 1840–1851, doi:10.1002/jgrd.50176, 2013.
605
- 606 Flanner, M. G., Zender, C. S., Randerson, J. T., and Rasch, P. J.: Present day
607 climate forcing and response from black carbon in snow, *J. Geophys. Res.*, 112,
608 D11202, doi:10.1029/2006JD008003, 2007.
609
- 610 Geoffroy, O., Saint-Martin, D., Bellon, G., Voldoire, A., Olivie, D. J., and Tytca, S.:
611 Transient climate response in a two-layer energy-balance model. Part II:
612 Representation of the efficacy of deep-ocean heat uptake and validation for
613 CMIP5 AOGCMs, *J. Climate*, 26, 1859–1876, doi:10.1175/JCLI-D-12-00196.1,
614 2013.
615
- 616 Gettelman, A., Liu, X., Ghan, S. J., Morrison, H., Park, S., Conley, A. J., Klein, S. A.,
617 Boyle, J., Mitchell, D. L., and Li, J. L. F.: Global simulations of ice nucleation and
618 ice supersaturation with an improved cloud scheme in the Community
619 Atmosphere Model, *J. Geophys. Res.*, 115, D18216, doi:10.1029/2009jd013797,
620 2010.
621
- 622 Ghan, S. J.: Technical Note: Estimating aerosol effects on cloud radiative forcing,
623 *Atmos. Chem. Phys.*, 13, 9971–9974, doi:10.5194/acp-13-9971-2013, 2013.
624
- 625 Hansen, J., Sato, M., Ruedy, R., Nazarenko, L., Lacis, A., Schmidt, G. A., Russell, G.,
626 Aleinov, I., Bauer, M., Bauer, S., Bell, N., Cairns, B., Canuto, V., Chandler, M.,
627 Cheng, Y., Del Genio, A., Faluvegi, G., Fleming, E., Friend, A., Hall, T., Jackman,
628 C., Kell, M., Kiang, N., Koch, D., Lean, J., Lerner, J., Lo, K., Menon, S., Miller,
629 R., Minnis, P., Novakov, T., Oinas, V., Perlwitz, Ja., Perlwitz, Ju., Rind, D.,
630 Romanou, A., Shindell, D., Stone, P., Sun, S., Tausnev, N., Thresher, D., Wielicki,
631 B., Wong, T., Yao, M., and Zhang, S.: Efficacy of climate forcings, *J. Geophys.*
632 *Res.*, 110, D18104, doi:10.1029/2005JD005776, 2005.
633
- 634 Hoesly, R. M., Smith, S. J., Feng, L., Klimont, Z., Janssens-Maenhout, G., Pitkanen,
635 T., Seibert, J. J., Vu, L., Andres, R. J., Bolt, R. M., Bond, T. C., Dawidowski, L.,
636 Kholod, N., Kurokawa, J.-I., Li, M., Liu, L., Lu, Z., Moura, M. C. P., O'Rourke, P.
637 R., and Zhang, Q.: Historical (1750–2014) anthropogenic emissions of reactive
638 gases and aerosols from the Community Emissions Data System (CEDS),
639 *Geosci. Model Dev.*, 11, 369–408, doi:10.5194/gmd-11-369-2018, 2018.
640
- 641 Hurrell, J. W., Holland, M. M., Gent, P. R., Ghan, S., Kay, J. E., Kushner, P. J.,
642 Lamarque, J. F., Large, W. G., Lawrence, D., Lindsay, K., Lipscomb, W. H., Long,
643 M. C., Mahowald, N., Marsh, D. R., Neale, R. B., Rasch, P., Vavrus, S.,



- 644 Vertenstein, M., Bader, D., Collins, W. D., Hack, J. J., Kiehl, J., and Marshall, S.:
645 The Community Earth System Model A Framework for Collaborative Research, B.
646 Am. Meteorol. Soc., 94, 1339–1360, doi:10.1175/BAMS-D-12-00121.1, 2013.
647
- 648 Hwang, Y.-T., Frierson, D. M. W., and Kang, S. M.: Anthropogenic sulfate aerosol
649 and the southward shift of tropical precipitation in the late 20th century, Geophys.
650 Res. Lett., 40, 2845–2850, doi:10.1002/grl.50502, 2013.
651
- 652 Jacobson, M. Z.: Climate response of fossil fuel and biofuel soot, accounting for
653 soot's feedback to snow and sea ice albedo and emissivity, J. Geophys. Res.,
654 109, D21201, doi:10.1029/2004JD004945, 2004.
655
- 656 Johnson, B. T., Shine, K. P., and Forster, P. M.: The semi-direct aerosol effect:
657 Impact of absorbing aerosols on marine stratocumulus, Q. J. Roy. Meteor. Soc.,
658 130, 1407–1422, doi:10.1256/qj.03.61, 2004.
659
- 660 Koch, D. and Del Genio, A. D.: Black carbon semi-direct effects on cloud cover:
661 review and synthesis, Atmos. Chem. Phys., 10, 7685–7696,
662 doi:10.5194/acp-10-7685-2010, 2010.
663
- 664 Koren, I., Kaufman, Y. J., Remer, L. A., and Martins, J. V.: Measurement of the effect
665 of Amazon smoke on inhibition of cloud formation, Science, 303, 1342–1345, doi:
666 10.1126/science.1089424, 2004.
667
- 668 Kvalevåg, M. M., Samset, B. H., and Myhre, G.: Hydrological sensitivity to
669 greenhouse gases and aerosols in a global climate model, Geophys. Res. Lett.,
670 40, 1432–1438, doi:10.1002/grl.50318, 2013.
671
- 672 Liu, X., Ma, P.-L., Wang, H., Tilmes, S., Singh, B., Easter, R. C., Ghan, S. J., and
673 Rasch, P. J.: Description and evaluation of a new four-mode version of the Modal
674 Aerosol Module (MAM4) within version 5.3 of the Community Atmosphere Model,
675 Geosci. Model Dev., 9, 505–522, doi:10.5194/gmd-9-505-2016, 2016.
676
- 677 McFarquhar, G. M., Ghan, S., Verlinde, J., Korolev, A., Strapp, J. W., Schmid, B.,
678 Tomlinson, J. M., Wolde, M., Brooks, S. D., Cziczo, D., Dubey, M. K., Fan, J.,
679 Flynn, C., Gultepe, I., Hubbe, J., Gilles, M. K., Laskin, A., Lawson, P., Leaitch, W.
680 R., Liu, P., Liu, X., Lubin, D., Mazzoleni, C., Macdonald, A.-M., Moffet, R. C.,
681 Morrison, H., Ovchinnikov, M., Shupe, M. D., Turner, D. D., Xie, S., Zelenyuk, A.,
682 Bae, K., Freer, M., and Glen, A.: Indirect and Semi-Direct Aerosol Campaign
683 (ISDAC): The Impact of Arctic Aerosols on Clouds, B. Am. Meteorol. Soc., 92,
684 183–201, doi:10.1175/2010BAMS2935.1, 2011.
685



- 686 McFarquhar, G. M. and Wang, H.: Effects of Aerosols on Trade Wind Cumuli over the
687 Indian Ocean: Model Simulations, *Q. J. R. Meteorol. Soc.*, 132, 821–843,
688 doi:10.1256/qj.04.179, 2006.
689
- 690 Ming, Y., Ramaswamy, V., and Persad, G.: Two opposing effects of absorbing
691 aerosols on global-mean precipitation, *Geophys. Res. Lett.*, 37, L13701,
692 doi:10.1029/2010GL042895, 2010.
693
- 694 Morrison, H. and Gettelman, A.: A new two-moment bulk stratiform cloud
695 microphysics scheme in the Community Atmosphere Model, version 3 (CAM3),
696 Part I: Description and numerical tests, *J. Clim.*, 21, 3642–3659,
697 doi:10.1175/2008JCLI2105.1, 2008.
698
- 699 Oshima, N., Koike, M., Zhang, Y., Kondo, Y., Moteki, N., Takegawa, N., and Miyazaki,
700 Y.: Aging of black carbon in outflow from anthropogenic sources using a mixing
701 state resolved model: Model development and evaluation, *J. Geophys. Res.*, 114,
702 D06210, doi: 10.1029/2008JD010680, 2009.
703
- 704 Qian, Y., Wang, H., Zhang, R., Flanner, M. G., and Rasch, P. J.: A sensitivity study on
705 modeling black carbon in snow and its radiative forcing over the Arctic and
706 Northern China, *Environ. Res. Lett.*, 9, 064001,
707 doi:10.1088/1748-9326/9/6/064001, 2014.
708
- 709 Ramanathan, V. and Carmichael, G.: Global and regional climate changes due to
710 black carbon, *Nat. Geosci.*, 1, 221–227, doi:10.1038/ngeo156, 2008.
711
- 712 Sand, M., Berntsen, T. K., Kay, J. E., Lamarque, J. F., Seland, Ø., and Kirkevåg, A.:
713 The Arctic response to remote and local forcing of black carbon, *Atmos. Chem.*
714 *Phys.*, 13, 211–224, doi:10.5194/acp-13-211-2013, 2013a.
715
- 716 Sand, M., Berntsen, T. K., Seland, Ø., and Kristjánsson, J. E.: Arctic surface
717 temperature change to emissions of black carbon within Arctic or midlatitudes, *J.*
718 *Geophys. Res. Atmos.*, 118, 7788–7798, doi:10.1002/jgrd.50613, 2013b.
719
- 720 Sand, M., Iversen, T., Bohlinger, P., Kirkevåg, A., Seierstad, I., Seland, Ø., and
721 Sorteberg, A.: A standardized global climate model study showing unique
722 properties for the climate response to black carbon aerosols, *J. Climate.*, 28,
723 2512–2526, doi:10.1175/JCLI-D-14-00050.1, 2015.
724
- 725 Sand, M., Berntsen, T. K., von Salzen, K., Flanner, M. G., Langner, J., and Victor, D.
726 G.: Response of Arctic temperature to changes in emissions of short-lived climate
727 forcers, *Nat. Clim. Change*, 6, 286–289, doi:10.1038/nclimate2880, 2016.
728



- 729 Shindell, D., Kuylenstierna, J. C. I., Vignati, E., van Dingenen, R., Amann, M., Klimont,
730 Z., Anenberg, S. C., Muller, N., Janssens-Maenhout, G., Raes, F., Schwartz, J.,
731 Faluvegi, G., Pozzoli, L., Kupiainen, K., Höglund-Isaksson, L., Emberson, L.,
732 Streets, D., Ramanathan, V., Hicks, K., Oanh, N. T. K., Milly, G., Williams, M.,
733 Demkine, V., and Fowler, D.: Simultaneously Mitigating Near-Term Climate
734 Change and Improving Human Health and Food Security, *Science*, 335, 183–189,
735 doi:10.1126/science.1210026, 2012.
- 736
- 737 Smith, S. J. and Mizrahi, A.: Near-term climate mitigation by short-lived forcers, *Proc.*
738 *Natl. Acad. Sci.*, 110, 14202–14206, doi:10.1073/pnas.1308470110, 2013.
- 739
- 740 Stjern, C. W., Samset, B. H., Myhre, G., Forster, P. M., Hodnebrog, Ø., Andrews, T.,
741 Boucher, O., Faluvegi, G., Iversen, T., Kasoar, M., Kharin, V., Kirkevåg, A.,
742 Lamarque, J.-F., Olivieì, D., Richardson, T., Shawki, D., Shindell, D., Smith, C.,
743 Takemura, T., and Voulgarakis, A.: Rapid adjustments cause weak surface
744 temperature response to increased black carbon concentrations, *J. Geophys.*
745 *Res. Atmos.*, 122, 11462–11481, doi:10.1002/2017JD027326, 2017.
- 746
- 747 Shindell, D. and Faluvegi, G.: Climate response to regional radiative forcing during
748 the twentieth century, *Nat. Geosci.*, 2, 294–300, doi:10.1038/ngeo473, 2009.
- 749
- 750 van Marle, M. J. E., Kloster, S., Magi, B. I., Marlon, J. R., Daniau, A.-L., Field, R. D.,
751 Arneeth, A., Forrest, M., Hantson, S., Kehrwald, N. M., Knorr, W., Lasslop, G., Li,
752 F., Mangeon, S., Yue, C., Kaiser, J. W., and van der Werf, G. R.: Historic global
753 biomass burning emissions for CMIP6 (BB4CMIP) based on merging satellite
754 observations with proxies and fire models (1750–2015), *Geosci. Model Dev.*, 10,
755 3329–3357, doi:10.5194/gmd-10-3329-2017, 2017.
- 756
- 757 Wang, H., Easter, R. C., Rasch, P. J., Wang, M., Liu, X., Ghan, S. J., Qian, Y., Yoon,
758 J.-H., Ma, P.-L., and Vinoj, V.: Sensitivity of remote aerosol distributions to
759 representation of cloud–aerosol interactions in a global climate model, *Geosci.*
760 *Model Dev.*, 6, 765–782, doi:10.5194/gmd-6-765-2013, 2013.
- 761
- 762 Wang, M., Larson, V., Ghan, S., Ovchinnikov, M., Schanen, D., Xiao, H., Liu, X., Guo,
763 Z., and Rasch, P.: A multiscale modeling framework model (superparameterized
764 CAM5) with a higher-order turbulence closure: Model description and low-cloud
765 simulations, *J. Adv. Model. Earth Syst.*, 7, 484–509, doi:10.1002/2014MS000375,
766 2015.
- 767
- 768 Yang, Y., Wang, H., Smith, S. J., Ma, P.-L., and Rasch, P. J.: Source attribution of
769 black carbon and its direct radiative forcing in China, *Atmos. Chem. Phys.*, 17,
770 4319–4336, doi:10.5194/acp-17-4319-2017, 2017.
- 771



- 772 Yang, Y., Wang, H., Smith, S. J., Zhang, R., Lou, S., Qian, Y., Ma, P.-L., Rasch, P. J.:
773 Recent intensification of winter haze in China linked to foreign emissions and
774 meteorology, *Sci. Rep.*, 8, 2107, doi:10.1038/s41598-018-20437-7, 2018a.
775
- 776 Yang, Y., Wang, H., Smith, S. J., Zhang, R., Lou, S., Yu, H., Li, C., and Rasch, P. J.:
777 Source apportionments of aerosols and their direct radiative forcing and
778 long-term trends over continental United States, *Earth's Future*, 6, 793–808,
779 doi:10.1029/2018EF000859, 2018b.
780
- 781 Yang, Y., Wang, H., Smith, S. J., Easter, R. C., and Rasch, P. J.: Sulfate aerosol in
782 the Arctic: Source attribution and radiative forcing, *J. Geophys. Res. Atmos.*, 123,
783 1899–1918, doi:10.1002/2017JD027298, 2018c.
784
- 785 Zhang, R., Wang, H., Hegg, D. A., Qian, Y., Doherty, S. J., Dang, C., Ma, P.-L.,
786 Rasch, P. J., and Fu, Q.: Quantifying sources of black carbon in western North
787 America using observationally based analysis and an emission tagging technique
788 in the Community Atmosphere Model, *Atmos. Chem. Phys.*, 15, 12805–12822,
789 doi:10.5194/acp-15-12805-2015, 2015a.
790
- 791 Zhang, R., Wang, H., Qian, Y., Rasch, P. J., Easter, R. C., Ma, P.-L., Singh, B.,
792 Huang, J., and Fu, Q.: Quantifying sources, transport, deposition, and radiative
793 forcing of black carbon over the Himalayas and Tibetan Plateau, *Atmos. Chem.*
794 *Phys.*, 15, 6205–6223, doi:10.5194/acp-15-6205-2015, 2015b.
795



796 **Table 1.** Changes in black carbon (BC) column burden, direct radiative effect (DRE)
 797 and cloud radiative effect (CRE) at the top of the atmosphere (TOA), surface BC
 798 snow/ice-albedo forcing, surface temperature (T) and total precipitation rate (P,
 799 including rain and snow) averaged over the Arctic (60–90°N), mid-latitudes (28–60°N)
 800 and the globe between perturbed (ARC150X/MID7X) and PD simulations. BC burden,
 801 DRE, CRE, and snow/ice-albedo forcing efficiencies, T sensitivity and P sensitivity
 802 are calculated as changes in regional mean BC column burden, DRE, CRE,
 803 snow/ice-albedo forcing, T and P divided by changes in global total BC emissions
 804 between perturbed and PD simulations, respectively. 1- σ for 80-annual means is
 805 shown in the parentheses. Note that these quantities include the impact of slow
 806 responses and feedbacks (e.g., changes in sea surface temperature and sea ice and
 807 feedbacks with clouds) so are not strictly comparable to the conventional definition of
 808 radiative forcing.
 809

	Δ Column Burden (mg m^{-2})			Burden Eff. ($\text{mg m}^{-2} (\text{Tg yr}^{-1})^{-1}$)			Δ DRE (W m^{-2})		
	60–90°N	28–60°N	Global	60–90°N	28–60°N	Global	60–90°N	28–60°N	Global
ARC150X	5.37 (± 0.30)	1.34 (± 0.05)	0.63 (± 0.03)	0.425 (± 0.024)	0.106 (± 0.004)	0.050 (± 0.002)	3.94 (± 0.39)	0.83 (± 0.04)	0.45 (± 0.03)
MID7X	2.19 (± 0.09)	3.97 (± 0.09)	1.26 (± 0.03)	0.106 (± 0.004)	0.191 (± 0.004)	0.061 (± 0.001)	2.90 (± 0.19)	2.49 (± 0.09)	1.00 (± 0.04)
	DRE Eff. ($\text{W m}^{-2} (\text{Tg yr}^{-1})^{-1}$)			Δ CRE (W m^{-2})			CRE Eff. ($\text{W m}^{-2} (\text{Tg yr}^{-1})^{-1}$)		
	60–90°N	28–60°N	Global	60–90°N	28–60°N	Global	60–90°N	28–60°N	Global
ARC150X	0.39 (± 0.03)	0.11 (± 0.00)	0.05 (± 0.00)	-3.83 (± 0.98)	-0.46 (± 0.84)	-0.22 (± 0.54)	-0.30 (± 0.08)	-0.04 (± 0.07)	-0.02 (± 0.04)
MID7X	0.17 (± 0.01)	0.22 (± 0.01)	0.08 (± 0.00)	-2.30 (± 0.96)	-3.16 (± 0.90)	-1.26 (± 0.51)	-0.11 (± 0.05)	-0.15 (± 0.04)	-0.06 (± 0.02)
	Δ Snow/ice-albedo Forcing (W m^{-2})			Snow/ice-albedo Eff. ($\text{W m}^{-2} (\text{Tg yr}^{-1})^{-1}$)			Δ T (K)		
	60–90°N	28–60°N	Global	60–90°N	28–60°N	Global	60–90°N	28–60°N	Global
ARC150X	1.26 (± 0.08)	0.12 (± 0.02)	0.10 (± 0.01)	0.099 (± 0.006)	0.010 (± 0.002)	0.008 (± 0.001)	2.13 (± 0.65)	0.78 (± 0.22)	0.48 (± 0.26)
MID7X	0.53 (± 0.05)	0.18 (± 0.03)	0.07 (± 0.01)	0.026 (± 0.002)	0.009 (± 0.001)	0.003 (± 0.000)	0.48 (± 0.79)	0.45 (± 0.27)	0.23 (± 0.26)
	T Sensitivity ($\text{K} (\text{Tg yr}^{-1})^{-1}$)			Δ P (mm day^{-1})			P Sensitivity ($\mu\text{m day}^{-1} (\text{Tg yr}^{-1})^{-1}$)		
	60–90°N	28–60°N	Global	60–90°N	28–60°N	Global	60–90°N	28–60°N	Global
ARC150X	0.169 (± 0.052)	0.062 (± 0.018)	0.038 (± 0.020)	-0.043 (± 0.079)	-0.011 (± 0.066)	0.010 (± 0.023)	-3.38 (± 6.29)	-0.86 (± 5.26)	0.77 (± 1.84)
MID7X	0.023 (± 0.038)	0.022 (± 0.013)	0.011 (± 0.012)	0.048 (± 0.096)	-0.159 (± 0.069)	-0.032 (± 0.022)	2.34 (± 4.61)	-7.67 (± 3.34)	-1.52 (± 1.04)

810

811



812 **Table 2.** BC burden, DRE, CRE, and snow/ice-albedo forcing efficiencies, T
 813 sensitivity and P sensitivity over the Arctic (60–90°N), mid-latitudes (28–60°N) and
 814 the globe between perturbed (ARC75X/ARC150X/MID3.5X/MID7X/MID14X) and PD
 815 simulations. 1- σ for 80-annual means is shown in the parentheses.
 816

	ARC75X	ARC150X		MID3P5X	MID7X	MID14X
	Burden Eff. ($\text{mg m}^{-2} (\text{Tg yr}^{-1})^{-1}$)					
60–90°N	0.406 (± 0.021)	0.425 (± 0.024)		0.095 (± 0.005)	0.106 (± 0.004)	0.124 (± 0.004)
28–60°N	0.097 (± 0.004)	0.106 (± 0.004)		0.175 (± 0.005)	0.191 (± 0.004)	0.219 (± 0.005)
Global	0.047 (± 0.002)	0.050 (± 0.002)		0.055 (± 0.001)	0.061 (± 0.001)	0.070 (± 0.002)
	DRE Eff. ($\text{W m}^{-2} (\text{Tg yr}^{-1})^{-1}$)					
60–90°N	0.346 (± 0.036)	0.312 (± 0.031)		0.146 (± 0.014)	0.140 (± 0.009)	0.137 (± 0.006)
28–60°N	0.069 (± 0.005)	0.066 (± 0.003)		0.129 (± 0.006)	0.120 (± 0.004)	0.112 (± 0.003)
Global	0.038 (± 0.003)	0.035 (± 0.003)		0.051 (± 0.003)	0.048 (± 0.002)	0.046 (± 0.001)
	CRE Eff. ($\text{W m}^{-2} (\text{Tg yr}^{-1})^{-1}$)					
60–90°N	-0.533 (± 0.232)	-0.303 (± 0.078)		-0.091 (± 0.166)	-0.111 (± 0.046)	-0.015 (± 0.029)
28–60°N	0.010 (± 0.222)	-0.037 (± 0.067)		0.070 (± 0.203)	-0.152 (± 0.043)	0.129 (± 0.035)
Global	-0.028 (± 0.071)	-0.017 (± 0.043)		0.013 (± 0.058)	-0.061 (± 0.025)	0.035 (± 0.010)
	Snow/ice-albedo Eff. ($\text{W m}^{-2} (\text{Tg yr}^{-1})^{-1}$)					
60–90°N	0.151 (± 0.011)	0.099 (± 0.006)		0.030 (± 0.003)	0.026 (± 0.002)	0.020 (± 0.002)
28–60°N	0.013 (± 0.003)	0.010 (± 0.002)		0.011 (± 0.002)	0.009 (± 0.001)	0.007 (± 0.001)
Global	0.012 (± 0.001)	0.008 (± 0.001)		0.004 (± 0.001)	0.003 (± 0.000)	0.003 (± 0.000)
	T Sensitivity ($\text{K} (\text{Tg yr}^{-1})^{-1}$)					
60–90°N	0.239 (± 0.116)	0.169 (± 0.052)		0.042 (± 0.098)	0.023 (± 0.038)	0.008 (± 0.015)
28–60°N	0.067 (± 0.032)	0.062 (± 0.018)		0.020 (± 0.025)	0.022 (± 0.013)	0.015 (± 0.005)
Global	0.040 (± 0.035)	0.038 (± 0.020)		0.008 (± 0.033)	0.011 (± 0.012)	0.005 (± 0.005)
	P Sensitivity ($\mu\text{m day}^{-1} (\text{Tg yr}^{-1})^{-1}$)					
60–90°N	-2.88 (± 13.39)	-3.38 (± 6.29)		1.73 (± 10.85)	2.34 (± 4.61)	1.86 (± 2.06)
28–60°N	-0.96 (± 9.45)	-0.86 (± 5.26)		-7.69 (± 8.90)	-7.67 (± 3.34)	-8.53 (± 1.61)
Global	0.31 (± 3.10)	0.77 (± 1.84)		-1.99 (± 2.81)	-1.52 (± 1.04)	-2.15 (± 0.49)

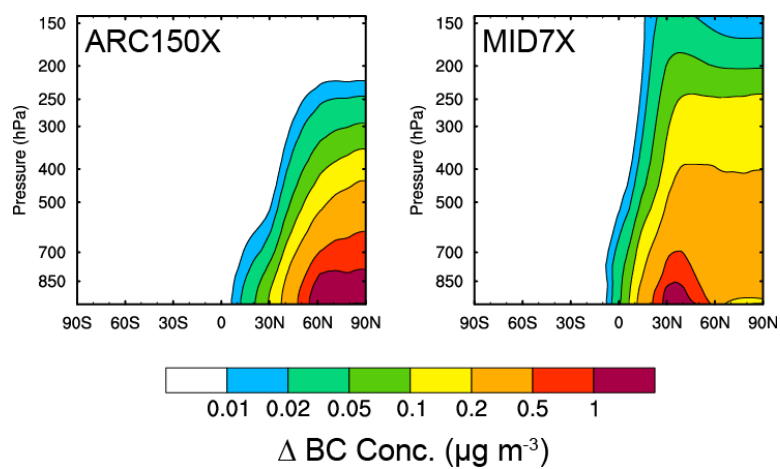
817

818



819 **Figures for Paper**

820



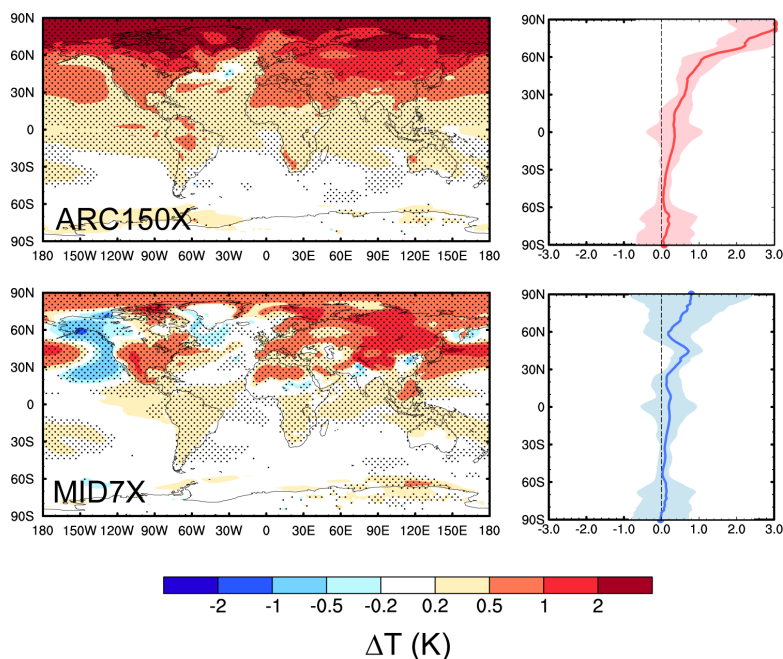
821

822

823 **Figure 1.** Difference in annual and zonal mean BC concentrations ($\mu\text{g m}^{-3}$) between
824 ARC150X (left)/MID7X (right) and PD simulations.

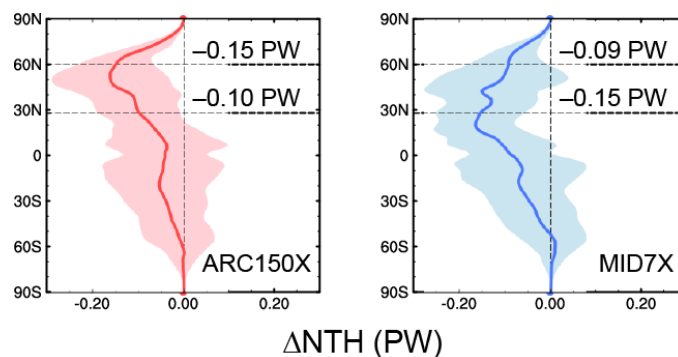
825

826



827
828
829
830
831
832
833
834
835
836

Figure 2. Spatial distribution (left) and zonal mean (right) of changes in annual mean surface air temperature (K) for ARC150X (top) and MID7X (bottom) compared to PD. The dotted areas in left panels indicate statistical significance with 95% confidence from a two-tailed Student's t test.



837

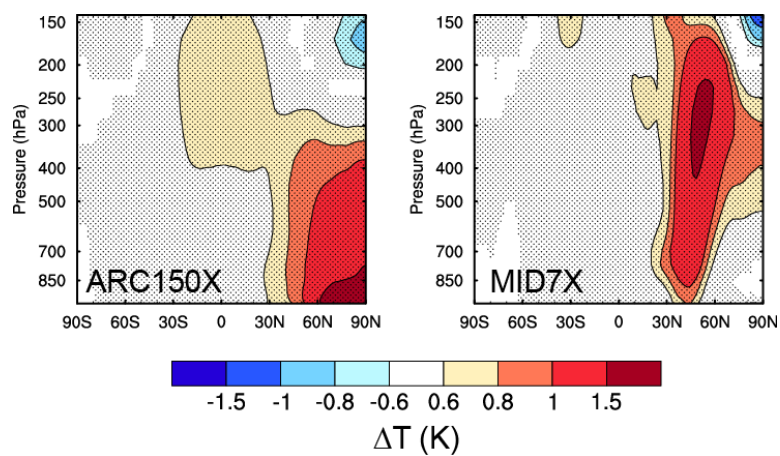
838

839 **Figure 3.** Zonal mean of changes in annual mean northward heat transport (NHT,
840 PW) for ARC150X (left) and MID7X (right) compared to PD. Values of changes in
841 NHT across 60°N and 28°N are shown in each panel. The shaded areas represent
842 1- σ for 80-annual means.

843

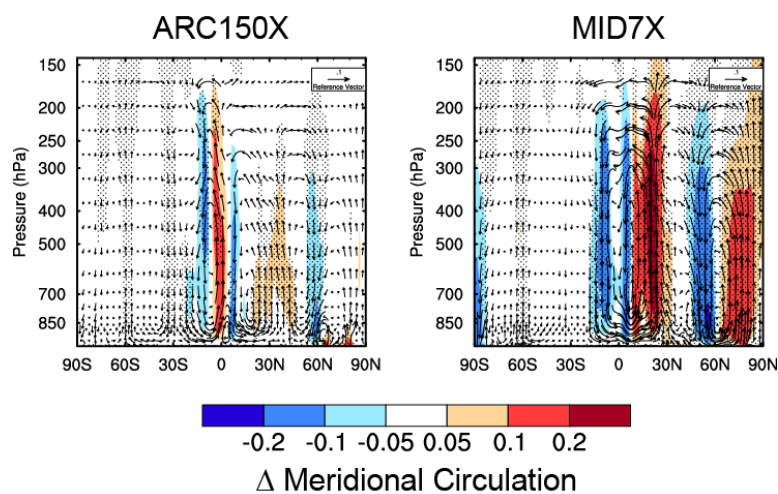
844

845



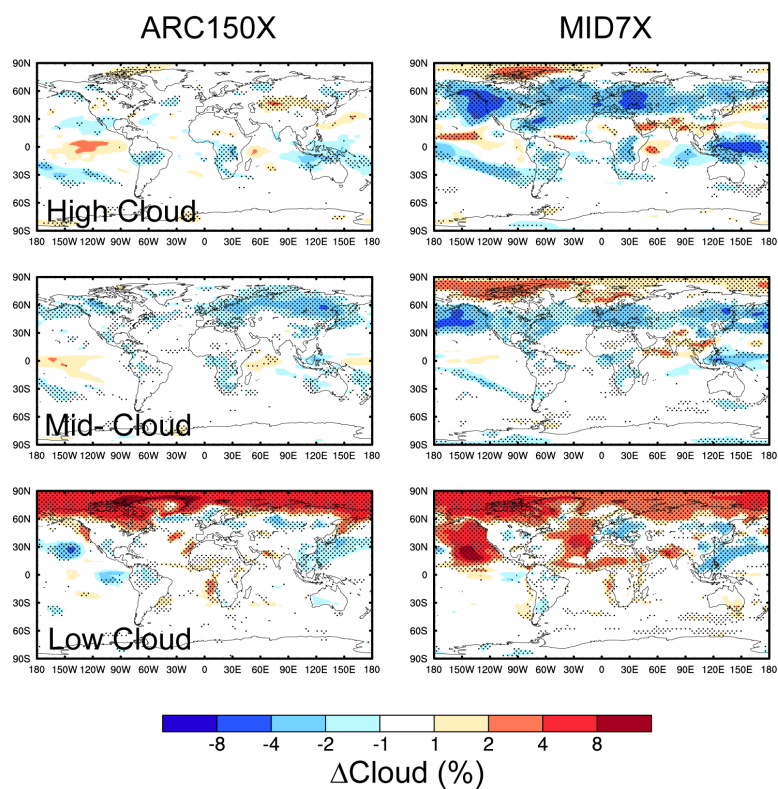
846
847
848
849
850
851
852

Figure 4. Changes in annual and zonal mean temperature (K) for ARC150X (left) and MID7X (right) compared to PD.



853
854
855
856
857
858
859

Figure 5. Changes in annual and zonal mean meridional wind vectors (m s^{-1}) and vertical velocity (contours; Pa s^{-1} scaled by a factor of -100) for ARC150X (left) and MID7X (right) compared to PD.



860

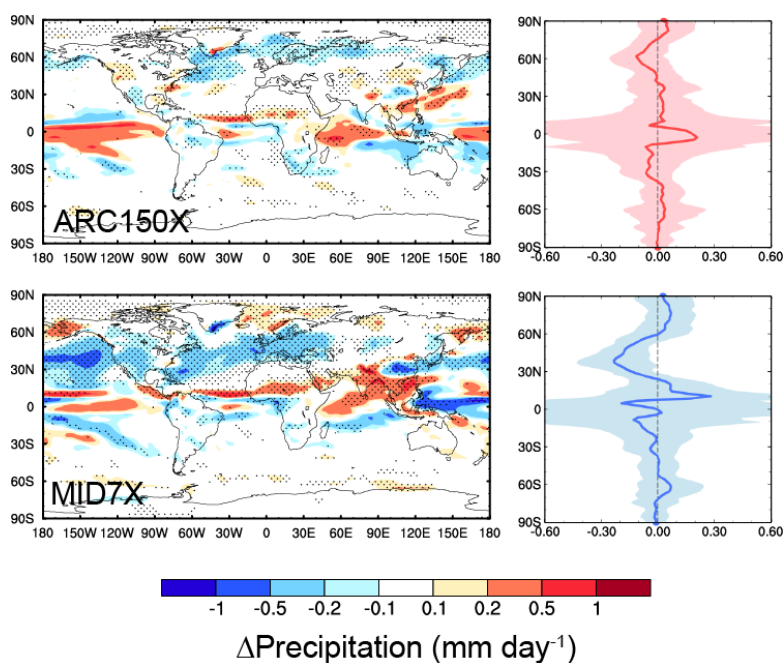
861

862 **Figure 6.** Changes in annual mean high (top), mid-level (middle), and low (bottom)
863 cloud fraction (%) for ARC150X (left) and MID7X (right) compared to PD.

864

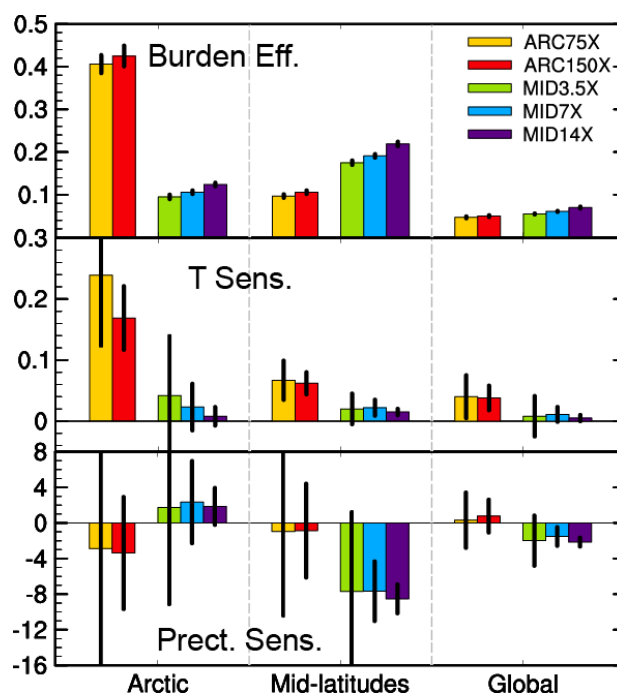
865

866



867
868
869
870
871
872
873

Figure 7. Spatial distribution (left) and zonal mean (right) of changes in annual mean total precipitation rate (mm day⁻¹) for ARC150X (top) and MID7X (bottom) compared to PD.



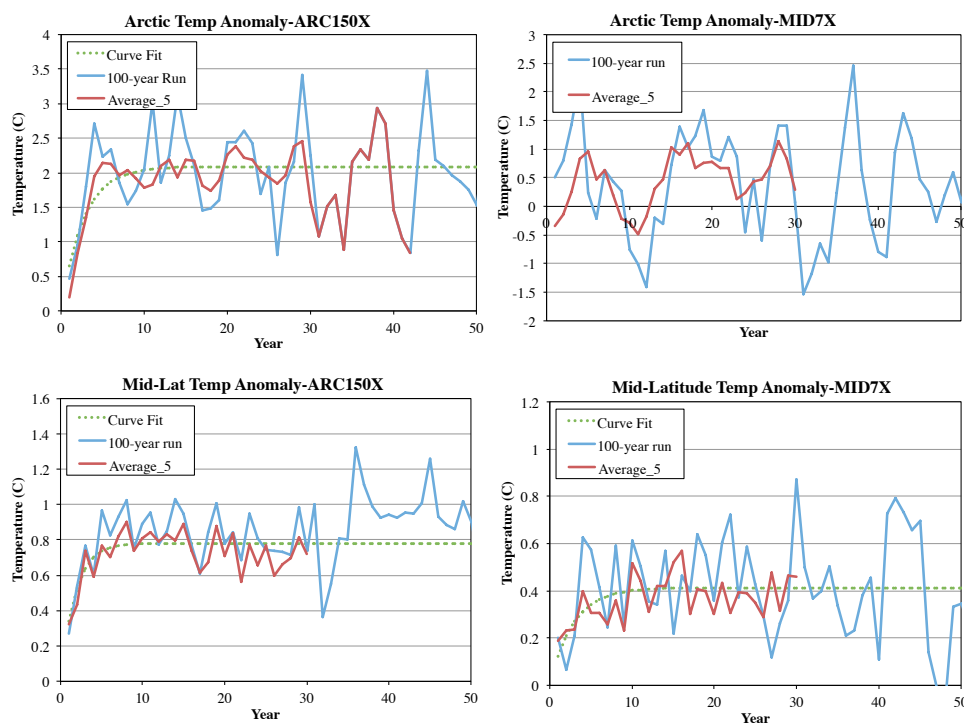
874

875

876 **Figure 8.** Burden efficiencies, temperature and precipitation sensitivities over the
877 Arctic, mid-latitudes and the whole globe for ARC75X, ARC150X, MID3.5X, MID7X
878 and MID14X. Burden efficiencies, temperature sensitivity and precipitation sensitivity
879 are calculated as changes in regional mean BC column burden, surface temperature
880 and total precipitation rate divided by changes in global total BC emissions between
881 perturbed and PD simulations, respectively. Error bars represent 1- σ for 80-annual
882 means.

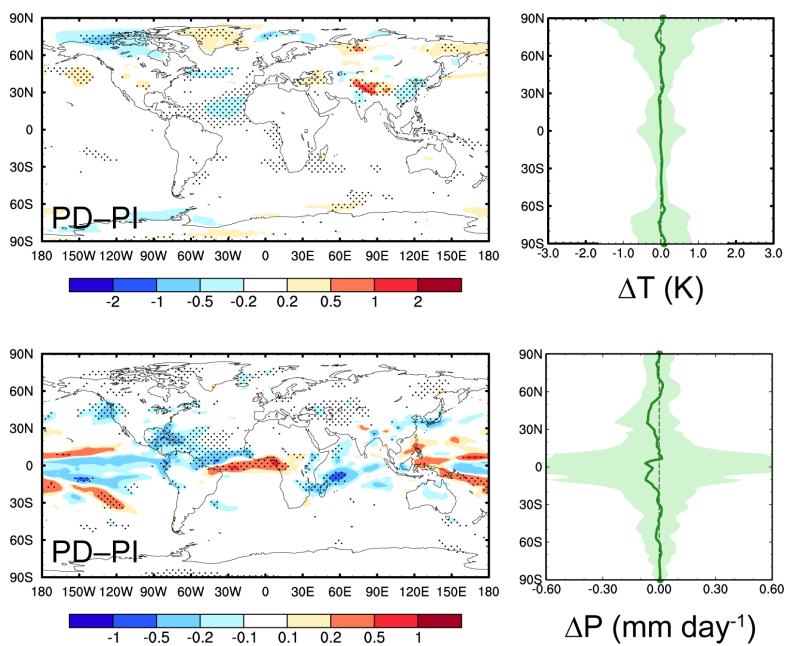
883

884



885
886
887
888
889
890
891
892
893
894
895
896
897
898

Figure 9. Time series of mean surface temperature response from ARC150X (left) and MID7X (right) BC emission perturbations as compared to PD. The response is shown over the Arctic (top) and mid-latitudes (bottom). Shown are the 100-year ensemble simulation (blue lines), the average of five 30-year ensemble members (red), and a numerical fit for an exponential approach to the long-term average (green dashed line). Curve fits used the package STAN in R, which is Bayesian inference using the No-U-Turn sampler. Note that MID7X Arctic temperature response does not result in a fit due to noise.



899
900
901
902
903
904
905

Figure 10. Spatial distribution (left) and zonal mean (right) of differences in annual mean surface temperature (K, top) and total precipitation rate (mm day^{-1} , bottom) between PD and PI.